Point-spread function of the ocean color bands of the Moderate Resolution Imaging Spectroradiometer on Aqua

Gerhard Meister* and Charles R. McClain

NASA Goddard Space Flight Center, Code 614.2, Greenbelt, Maryland 20771, USA

*Corresponding author: Gerhard.Meister@nasa.gov

Received 19 April 2010; revised 10 September 2010; accepted 28 September 2010; posted 5 October 2010 (Doc. ID 127042); published 5 November 2010

The Moderate Resolution Imaging Spectroradiometer (MODIS) on the Aqua platform has nine spectral bands with center wavelengths from 412 to 870 nm that are used to produce the standard ocean color data products. Ocean scenes usually contain high contrast due to the presence of bright clouds over dark water. About half of the MODIS Aqua ocean pixels are flagged as spatial stray light contaminated. The MODIS has been characterized for stray light effects prelaunch. In this paper, we derive point-spread functions for the MODIS Aqua ocean bands based on prelaunch line-spread function measurements. The stray light contamination of ocean scenes is evaluated based on artificial test scenes and on-orbit data. © 2010 Optical Society of America

OCIS codes: 290.1090, 290.2648, 290.5820, 280.4788, 110.3000.

1. Introduction

We present an estimate of the spatial stray light effects in the Moderate Resolution Imaging Spectroradiometer (MODIS) (see Barnes *et al.* [1]) on NASA's Earth Observing Systems (EOS) Aqua satellite [2]. The authors of this paper are part of NASA's Ocean Biology Production Group, which is responsible for producing ocean color products from MODIS on Aqua [3]. Therefore, the focus of this investigation is on the MODIS ocean color bands (MODIS bands 8–16, corresponding to wavelengths from 412 to 870 nm), which all have a nadir resolution of 1 km × 1 km.

MODIS is a scanning radiometer, with 10 detectors simultaneously recording for each ocean color band, resulting in 10 scan lines per scan. The MODIS optics are described by Waluschka *et al.* [4]. The first four optical surfaces are mirrors (scan, fold, primary, and secondary), with a field stop between the primary and the secondary mirrors. The three mirrors before the field stop are the fore-optics; the following optical elements the aft-optics. For bands 8–12, two beam splitters (in reflective mode) direct the light to the visible (VIS) focal plane, with three objective assembly lenses (E1, E2, E3) focusing the light onto the detectors. There are a total of nine optical elements in the light path to the VIS focal plane, and each element can produce scatter. The two largest sources for scatter are expected to be the first objective lens assembly, E1, and the primary mirror [5].

A point-spread function (PSF) is required to correct for stray light artifacts that are associated with contamination of the currently viewed pixel by light from outside the nominal field of view (FOV) of the current pixel. The PSF is defined here as

$$L_m(x_0,y_0) = \sum_{i,j} \mathrm{PSF}(i-x_0, j-y_0) \cdot L_T(i,j), \qquad (1)$$

where $L_m(x_0,y_0)$ is the measured radiance from pixel (x_0,y_0) and $L_T(i,j)$ is the true radiance of pixel (i,j). The first pixel index is for the scan direction [x_0 and i, 1–1354 in the case of MODIS; MODIS has 1354 1 km frames (or pixels) per scan line], the second for the track direction (y_0 and j, 1–2040 in a typical MODIS Level 1 B data file [6], also called "*granule*;" a typical

0003-6935/10/326276-10$15.00/0

MODIS granule contains 204 scans, so, for an ocean color band with 10 detectors, there are 2040 scan lines per granule). The summation should ideally cover all directions from which light enters the sensor but is, in practice, limited by the actual size of the image. The PSF is normalized to 1:

$$\sum_{i,j} \mathrm{PSF}(i,j) = 1. \tag{2}$$

The above definition is very similar to the definition used in Huang *et al.* [7]. However, the focus of Huang *et al.* was the stray light contamination for MODIS land bands directly adjacent to the stray light source, and they were interested in effects occurring at distances of less than 500 m. For the MODIS ocean bands, 1 km is the smallest usable distance to a stray light source (and, in the case of ocean next to a cloud, even the pixels directly adjacent to the cloud are so strongly contaminated by stray light that they are unusable), so the simplified PSF model used by Huang *et al.* cannot be applied to the ocean bands.

Zong *et al.* [8] developed a matrix-based correction approach for spectral stray light that allows the retrieval of the original image with relatively small computational cost. Recently, this approach was transferred to spatial stray light and successfully demonstrated for a CCD-array imaging radiometer [9]. Considering the enormous amounts of data produced by MODIS Aqua daily (about 35 Gbytes/day for Level 1B files with ocean color bands only), this approach could provide the opportunity for correcting all MODIS Aqua ocean color data for spatial stray light effects. However, a necessary requirement for an improvement in the resulting data set is that the sensor PSF is sufficiently well known. Unfortunately, the PSF was not directly measured by the instrument vendor, because NASA's instrument specifications for MODIS did not require this.

Sections 2 and 3 of this paper describe the PSF model creation for MODIS Aqua and Section 4 describes the resulting PSF. In Section 5, the PSF is applied to artificial scenes, showing that, even at a distance of 50 pixels from a large cloud, the correction can be significant. The intensity of the correction depends strongly on the size of the cloud and varies from band to band. Section 6 looks at cloud edge effects in real images.

2. Prelaunch Characterization

MODIS was characterized by Santa Barbara Remote Sensing (SBRS), California. Line-spread functions (LSFs) were acquired in two different modes:

1. varying the slit position by fractions of a pixel to determine the modulation transfer function (MTF), and
2. keeping the slit position constant, but inserting neutral density filters and measuring at different light intensities.

With the second method, the response of pixels far away from the slit measured with a high light intensity (so high that the slit measurements actually saturate) can be related to measurements of moderate light intensity without saturation. This type of LSF is called near-field response (NFR) by SBRS, see Hurt and Derrick [10]. The dynamic range of the MTF measurements is about 10^3; for the NFR measurements, it is about 10^7. To characterize the system response to a bright target located several pixels away, NFR measurements are needed. MODIS NFR was only characterized in the along-scan direction, not in the along-track direction. MODIS MTF was characterized for both directions.

The MODIS Aqua NFR measurements are described by Harvey–Shack functions by Derrick [11]. Harvey–Shack functions are often used to characterize the bidirectional reflectance function of specularly reflecting surfaces (see, e.g., [4,12]). The Harvey–Shack functions used by SBRS have the form

$$\rho = A \cdot \left(\frac{|(\sin(\theta + \phi_0) - \sin(\phi_0))|}{0.01} \right)^m \cdot (\mathrm{IFOV} \cdot \mathrm{mag})^2, \tag{3}$$

where ρ is the reflectance, θ is the scatter angle, and $\mathrm{IFOV} = 0.001418$ is the instantaneous FOV in radians. For the fore-optics, ϕ_0 is the incidence angle for the scan mirror, and $\mathrm{mag} = 1$ is the magnification. For the aft-optics, ϕ_0 is the incidence angle for the first beam splitter, and $\mathrm{mag} = 4$ is the magnification. The fit parameters A and m are called Harvey–Shack parameters and are provided for the individual optical surfaces in Waluschka *et al.* [4]. Note that the Harvey–Shack parameters for MODIS in Derrick [11] apply to the whole sensor, not its individual parts.

The model for MODIS was created by Young [13]. It predicts the measured response for pixels further than 1 pixel away from the slit. The model uses the sum of two Harvey–Shack functions if the direction of the incoming light is not blocked by the field stop (i.e., both fore- and aft-optics produce stray light that reaches the detector), but only one Harvey–Shack function if the direction of the incoming light is blocked by the field stop (i.e., only the aft-optics produces stray light that reaches the detector). This effect creates two distinct regions with different slopes on each side of the peak of the NFR measurements. Note that the position of the transition between the two regions is band dependent in the scan direction and detector dependent in the track direction, determined by the location of the band/detector relative to the field stop; see Figs. 1 and 2.

The parameters A and m of Eq. (3) were fitted by SBRS to the MODIS Aqua NFR measurements for both regions [11]. As an example, the results for band 11 are $A = 0.28$ and $m = -1.8$ for outside the field stop, and $A = 1.15$ and $m = -1.6$ for inside the field baffle. The NFR measurements are only available for

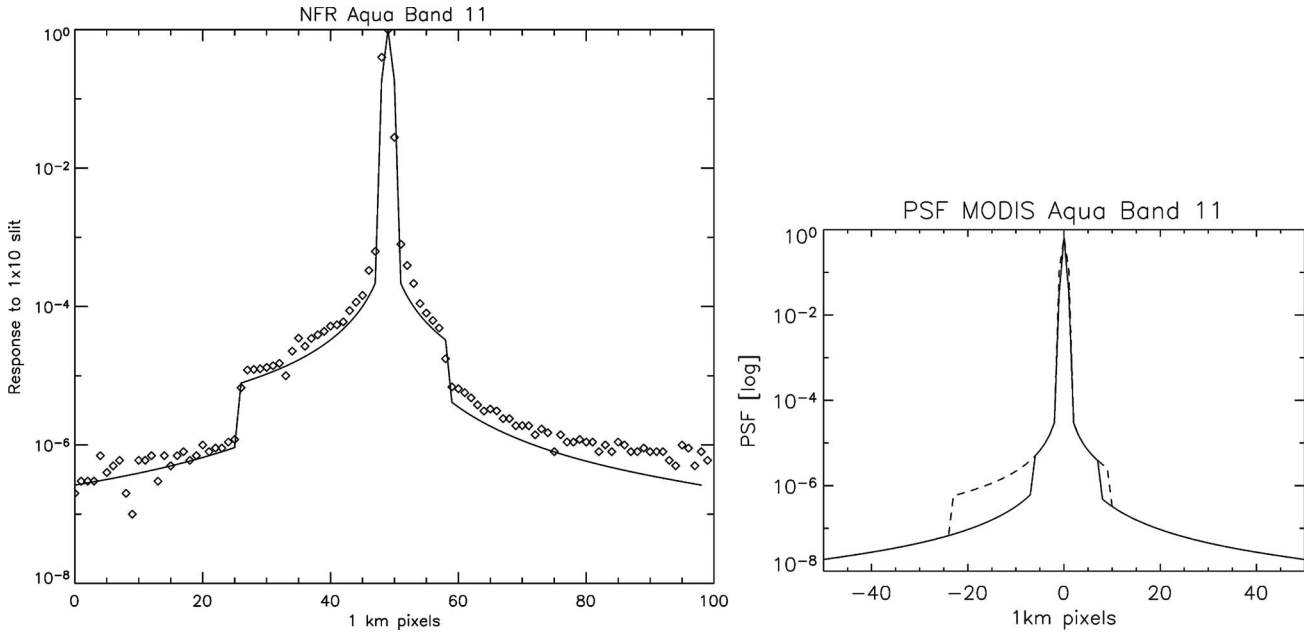

Fig. 1. Left, NFR measurements (diamonds) and NFR modeled from PSF (solid curve) for MODIS Aqua band 11. Right, MODIS Aqua band 11 PSF in track direction (solid curve) and scan direction (dashed curve).

detector 5, so we will assume that the Harvey–Shack coefficients of this detector are representative for all 10 detectors. The measured NFR values in Fig. 1 are slightly higher than the modeled values after the peak (right side of Fig. 1). Generally, data measured after the peak are less reliable due to hysteresis of the detectors and were not used in the fitting of the Harvey–Shack parameters by SBRS. The data points directly adjacent to the slit and the slit itself (i.e., the three central pixels in the scan direction) were not used in the fit; their inclusion into the PSF is described in the following section.

3. Derivation of the PSF

The general shape of the PSF is given by the Harvey–Shack-based model from SBRS. The along-track scattering Harvey–Shack parameters (which were not measured) are assumed to be identical to the along-scan parameters. The crucial step for the creation of the PSF from the SBRS model is the normalization of the central pixels relative to the SBRS model. The approach chosen here is to estimate the PSF of the central 3×3 pixels based on

- the LSFs in the along-track direction measured for the MTF characterization, and
- the theoretical value for the adjacent pixel in the scan direction without scattering.

The results are given in Table 1 as a function of $p_0 = \mathrm{PSF}(0,0)$, the value of the PSF for the central pixel (x_0, y_0), i.e., the maximum of the PSF. Without scattering, the preceding and following pixel in the scan direction measure 12.5% of the total energy [14], the central pixel 75%, so the preceding and following pixel each measure 0.125/0.75 of the intensity of the central pixel (about 17%); see Nishihama [15]. In the track direction, the preceding and subsequent pixels measure 5% of the intensity of the central pixel {according to prelaunch measurements, see Barnes *et al.* [1], Fig. 3(a)}. For completeness, we assume that the along-track scattering is similar even for the pixels that are not directly illuminated, so that the pixels which precede or follow the central pixels in the track direction (the corner pixels of the central 3×3 pixels, a total of four pixels) measure 5% of the theoretical value for the adjacent pixel in the scan direction, or about 0.8% $(0.05 \cdot 0.125/0.75)$.

The normalization constant p_0 is then optimized so that the resulting PSF reproduces the NFR measurements. Since the SBRS model is already optimized for the NFR measurements, this yields consistent PSF values for the central 3×3 pixels relative to the remaining pixels. As a last step, the PSF is normalized to 1 [see Eq. (2)].

4. Resulting PSF

The sum of the PSF of the central 3×3 pixels for MODIS Aqua band 11 is 0.9971. This means a fraction of $1.0 - 0.9971 = 0.0029$ (about 0.3%) is scattered into the remaining pixels. For MODIS Terra, Qiu *et al.* [5] reported a value of 0.9932 for band 11, i.e., significantly more $(1.0 - 0.9932 = 0.0068$, about 0.7%, i.e., more than double) scatter than we

Table 1. Modeled PSF of the 3×3 Central Pixels

Scan Index	Track Index	Value
0	0	p_0
±1	0	$0.125/0.75 \cdot p_0$
0	±1	$0.05 \cdot p_0$
±1	±1	$0.125/0.75 \cdot 0.05 \cdot p_0$

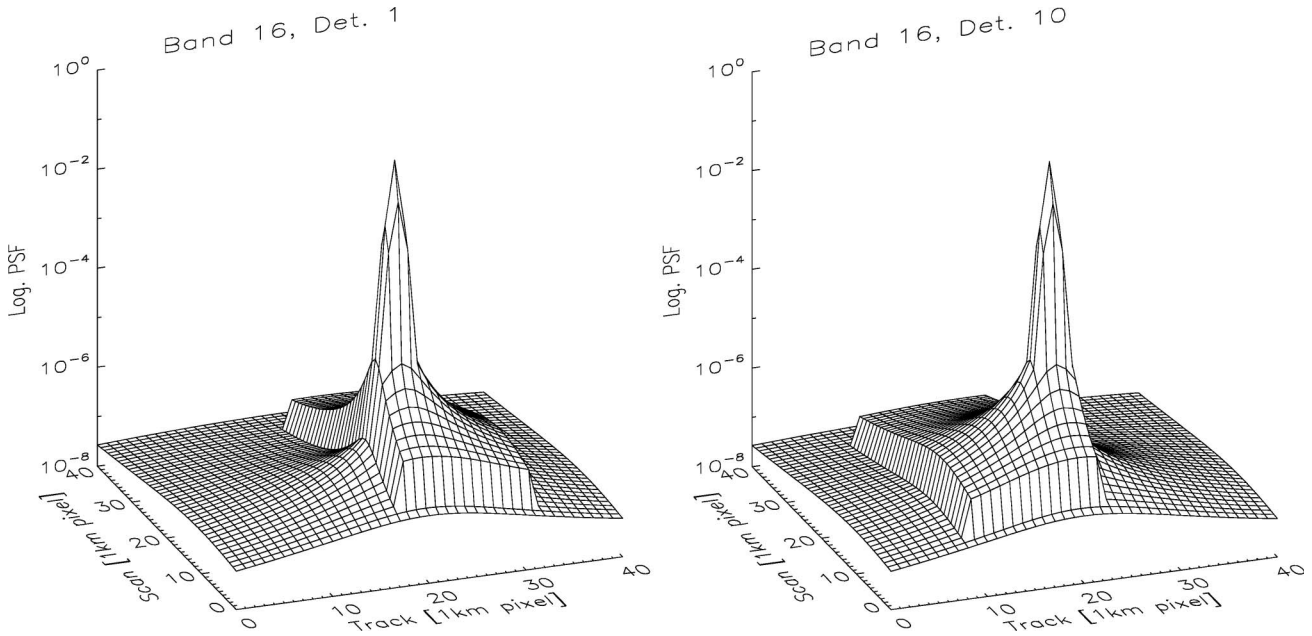

Fig. 2. Modeled MODIS Aqua PSF for band 16, detector 1 (left) and detector 10 (right).

find in MODIS Aqua. The agreement between modeled and measured NFR is shown in Fig. 1 for Aqua band 11; the modeled PSF is shown in Fig. 1 as well. All 10 detectors are assumed to have the same Harvey–Shack coefficients as detector 5, but their PSFs are different due to their different positions on the focal plane relative to the MODIS field baffle, which can be seen in Fig. 2. Note, also, that the position of the band on the focal plane influences its PSF: bands 11 and 16 are on different sides of the focal plane, and the PSF plateau in the scan direction is longer before the peak in band 11 (Fig. 1), but longer after the peak in band 16 (Fig. 2).

The equivalent of the NFR plot in Fig. 1 (left) has been shown in Qiu *et al.* [5] for MODIS Terra. Qualitatively, the NFR measurements of both MODIS instruments are similar, but the MODIS Aqua NFR measurements are generally lower, i.e., there is more stray light in MODIS Terra. This was expected, because the mirrors used in MODIS Aqua were of better quality than those in MODIS Terra.

The equivalent of the PSF plot in Fig. 1 (right) is also shown in Qiu *et al.* [5] for MODIS Terra. Thirty pixels away from the center peak, the PSF of MODIS Terra is a little less than 1×10^{-6}, whereas, for MODIS Aqua, it is 4.5×10^{-8}. Unfortunately, the PSF model used in Qiu *et al.* [5] is unavailable; the publication is the only source of information we can use.

5. Application to Test Images

Following the method outlined in Qiu *et al.* [5], an artificial image with 512×512 pixels was created with the left (or right) half of the image containing cloud radiances (Lcloud), and the other half containing typical radiances (Ltyp); see Fig. 3. Qiu did not define if the cloud is at the beginning of the scan or end of scan (EOS), so we calculated both cases (i.e., the cloud either in the left or the right half of the image). The PSF was applied to the artificial image to simulate the scattering of MODIS. The radiance error $L_e(x_0, y_0)$ of pixel (x_0, y_0) is the difference of the simulated image with scatter $L_m(x_0, y_0)$ and the artificial input image $L_T(x_0, y_0)$:

$$L_e(x_0, y_0) = L_m(x_0, y_0) - L_T(x_0, y_0), \tag{4}$$

where $L_m(x_0, y_0)$ is calculated with Eq. (1).

The radiance errors are shown in Fig. 4 as a function of (horizontal) distance to the cloud, evaluated along the center of the image (see dashed line in Fig. 3). A Lcloud/Ltyp ratio of exactly 20 was chosen in Fig. 4 to ensure comparability to data in Qiu *et al.* [5]. The values for MODIS Terra were read from the figure in Qiu *et al.* [5], and are, therefore, only approximate. It can be seen that the contamination of MODIS Aqua band 11 top-of-atmosphere (TOA) radiances due to a large cloud is significant (1% contamination 8 or 13 km away from the cloud, for the

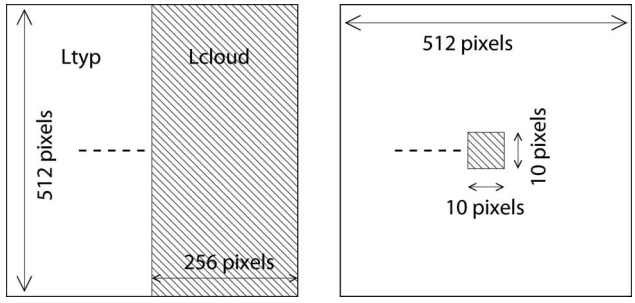

Fig. 3. Artificial test images used in Section 5: large cloud (left) and small cloud (right). Hatched areas indicate clouds. Dashed line shows location where radiance error was evaluated. Length of this line and size of small cloud are not to scale.

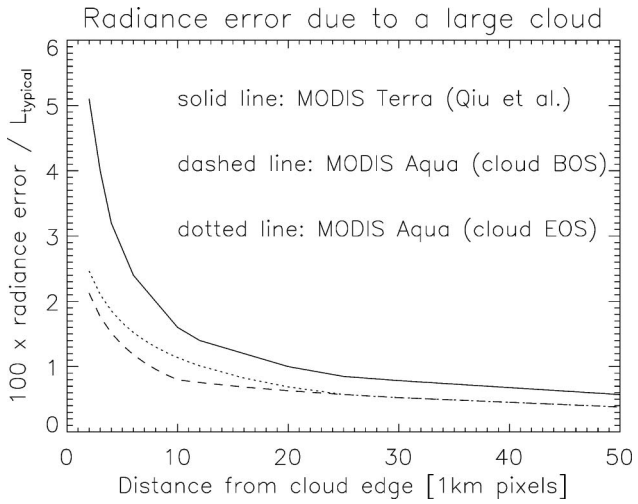

Fig. 4. Contamination of TOA radiances over ocean due to a large cloud (semi-infinite) for band 11. Ratio Lcloud/Ltyp is 20.

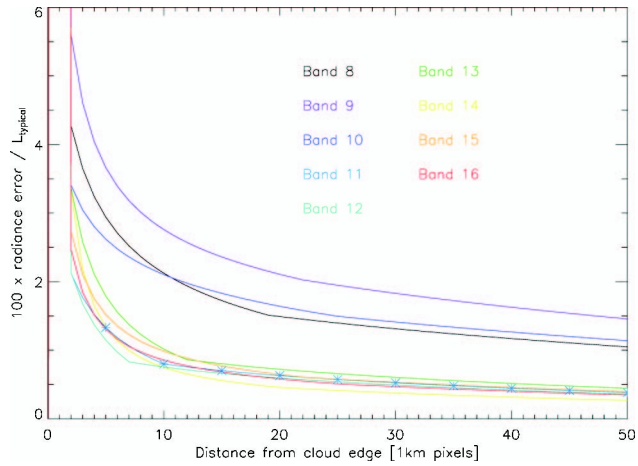

Fig. 5. Contamination of TOA radiances over ocean due to a large cloud (semi-infinite) for bands 8–16. The cloud is at the end of the scan (EOS). Stars indicate band 11 for better readability. Ratio Lcloud/Ltyp is 20 for all bands.

cloud being at the beginning or end of scan, respectively), but the contamination is much less than for MODIS Terra (1% contamination 21 pixels away from the cloud). Note that, 40 km away from the cloud, MODIS Terra contamination is about 50% higher than for MODIS Aqua, but 2 km away from the cloud, MODIS Terra is more than twice as high.

Figure 5 shows the expected response at the edge of a semi-infinite cloud for all MODIS Aqua bands, using a Lcloud/Ltyp ratio of 20 for all bands. Although this is not realistic, it shows the spectral dependence of the sensor inherent stray light effects due to the PSF very well. Bands 8–10 have the highest stray light effects for a constant ratio of Lcloud/Ltyp; bands 11–16 are all very similar.

A more realistic estimation of the stray light effects in ocean scenes uses the ratio of Lcloud/Ltyp (using the values from the MODIS specification document [16]) given in Table 2, and the results are shown in Fig. 6. Band 11 happens to be the band with the lowest stray light effects (10 pixels away from the cloud, L_e is 1.1% of Ltyp), and band 13 has by far the highest. Bands 15 and 16 have very similar stray light effects, which is an advantage for the ocean color atmospheric correction. Note that band 13 has a much stronger stray light response than band 14. This could be a problem for the fluorescence line height (FLH) algorithm, which critically depends on the radiance difference between those two bands. But it is not clear whether the stray light response difference between bands 13 and 14 is real or a characterization artifact, because it is surprising that the stray light characteristics are that different for two bands whose wavelengths are so close together (separated by 11 nm; see Table 2).

The cloud used in Figs. 4–6, is very large. The effect from a much smaller cloud (a single cloud of size 10 × 10 pixels with a radiance of Lcloud, inside an area of size 512 × 512 pixels with a radiance of Ltyp; see Fig. 3) can be seen in Fig. 7, using ratios Lcloud/Ltyp from Table 2. Ten pixels away from the cloud, the contamination is a little less than 0.3% for band 11.

The strong variation of stray light contamination among the bands is partly due to the different Lcloud/Ltyp ratios, and partly due to different PSFs (see the strong variation in the sum of the PSF of the central 3 × 3 pixels shown in Table 2). The between band variation is problematic for the ocean color products, because often stray light is removed from the ocean color products because it is (erroneously) characterized as aerosol contribution; the quality of the derived products suffers if the stray light contribution has a different wavelength dependency than the aerosol reflectance.

6. Cloud Edge Effects in Real Images

Stray light effects due to the sensor will appear in ocean images as elevated TOA radiances L_t of ocean pixels in the vicinity of clouds. It is important to note

Table 2. Specifications [16] for the MODIS Ocean Color Bands and Ratio of Sum of 3 × 3 Central PSF Pixels to Total PSF (i.e., Sum of PSF with 512 × 512 Elements) for MODIS Aqua[a]

Band	8	9	10	11	12	13	14	15	16
Center wavelength (nm)	412	443	488	531	551	667	678	748	869
Ltyp	44.9	41.9	32.1	27.9	21.0	9.5	8.7	10.2	6.2
Lcloud	573	585	539	538	528	471	440	373	286
Lcloud/Ltyp	12.8	14.0	16.8	19.3	25.1	49.6	46.3	36.6	46.1
PSF (3 × 3)/PSF (512 × 512)	0.9952	0.9933	0.9965	0.9973	0.9970	0.9956	0.9954	0.9967	0.9970

[a]Radiance units are W/(m^2 μm sr).

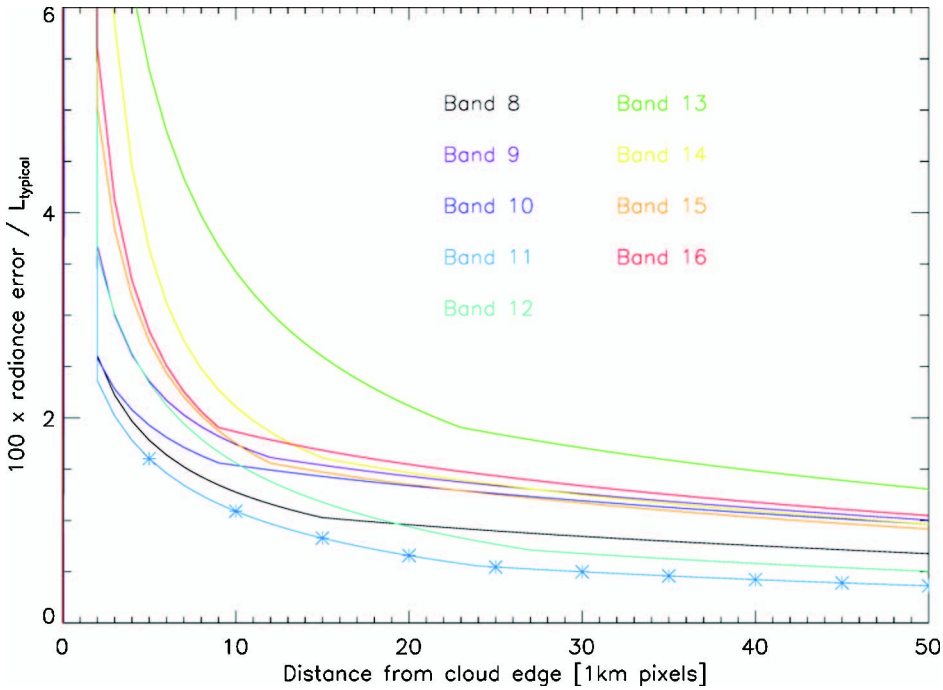

Fig. 6. Contamination of TOA radiances over ocean due to a large cloud (semi-infinite) for bands 8–16. The cloud is at the EOS. Stars indicate band 11 for better readability. Ratio Lcloud/Ltyp is taken from Table 2.

that a certain increase of L_t next to clouds is expected, e.g., due to scattering effects in the atmosphere or subpixel clouds. This increase is a topic of current scientific investigation [17–20].

As an initial step, a simple algorithm was used to quantify the increase of the radiances in the vicinity of clouds. Three MODIS granules (see Fig. 8) were processed with SeaDAS [21] from L1A data (uncalibrated digital numbers) to TOA radiances. One MODIS granule contains about 200 scans, or 2.75 million pixels. An ocean pixel is defined here as a pixel with a valid chlorophyll retrieval. The SeaDAS cloud flag was used to identify clouds, and it uses a TOA reflectance of 0.027 in band 16 as a threshold. Then the average radiance of all the ocean pixels adjacent to the cloud flag (either in the track or the scan direction, or diagonal) was calculated. These pixels were labeled with "Distance to cloud 1." Then all

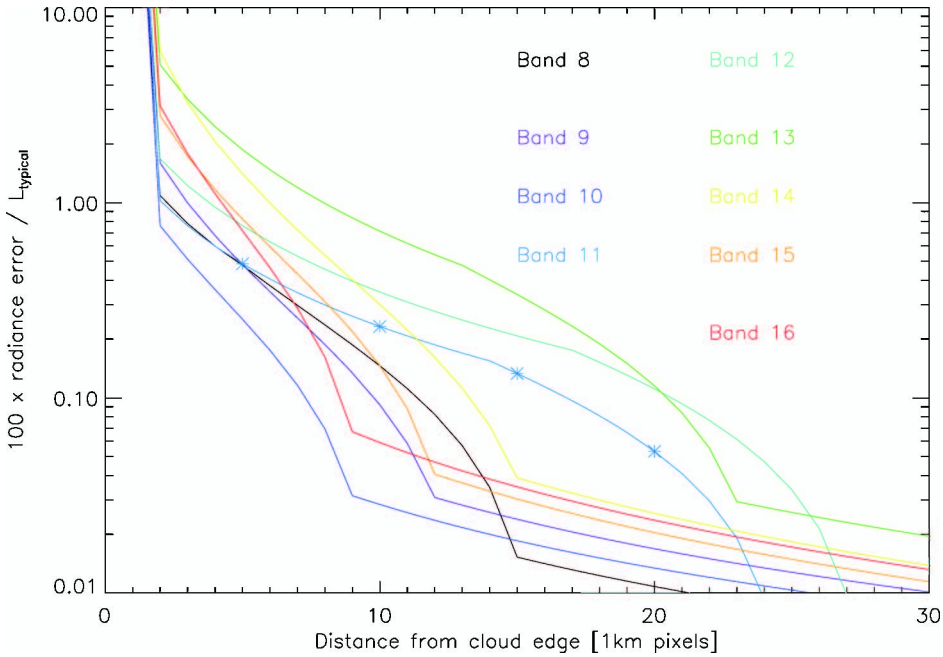

Fig. 7. Contamination of TOA radiances over ocean due to a small cloud (10 × 10 pixels) at the EOS. Ratio Lcloud/Ltyp is taken from Table 2.

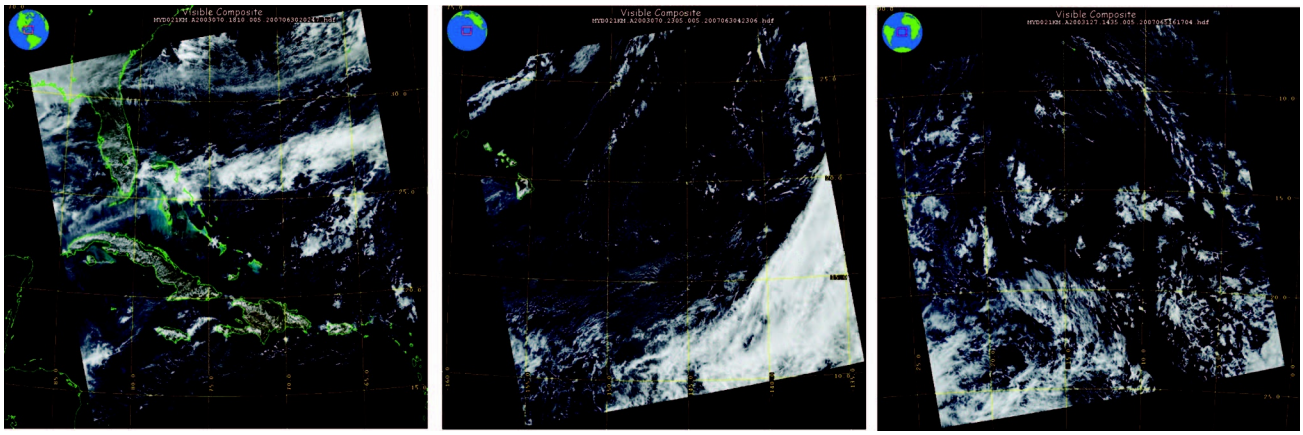

Fig. 8. Browse images for MODIS Aqua granules A20030701810, A20030702305, and 20031271435 (left to right), provided by LAADS Web (http://ladsweb.nascom.nasa.gov/).

the pixels adjacent to the pixels labeled "Distance to cloud 1" were identified, labeled "Distance to cloud 2," and their average was calculated. If a pixel was already labeled with "Distance to cloud 1" (because it was 1 pixel away from another cloud), it was not included in the second average. This was continued until "Distance to cloud 39." An example for the calculation of "Distance to cloud" is given in Fig. 9.

The number of pixels for each "Distance to cloud" is shown in Fig. 10 for each granule. It can be seen that most of the ocean pixels are actually very close to clouds (note the logarithmic scale). About half of the ocean pixels (e.g., 52% for all MODIS Aqua granules from 6 September 2002) are within a 5×7 mask around clouds. A 5×7 mask is used in the operational ocean color processing to flag stray light contaminated pixels; these pixels are not used to calculate level 3 data in the operational processing. Excluding those pixels, the average "Distance to cloud" is still about 12. So the true typical distance between a cloud edge and an unflagged ocean pixel is probably between 15 and 20 km, considering that (1) the "Distance to cloud" as defined here is actually a square and not a circle, and (2) the distance between pixels in the scan direction increases for high scan angles.

4	3	2	2	2	2
3	2	2	1	1	1
2	2	1	1		1
1	1	1			1
1		1	1	1	1

Fig. 9. Example of calculation of "Distance to cloud" for an area of 6×6 pixels with two distinct clouds. Hatched areas are pixels identified as clouds, numbers indicate "Distance to cloud" value for remaining pixels.

The average L_t for each set of pixels' "Distance to cloud x" (with $1 \le x < 40$) is shown in Fig. 11. It can be seen that the radiances increase significantly when approaching a cloud, by about 5% for the shorter wavelength bands and by up to 40% for the near-IR (NIR) bands. As noted above, this increase is most likely due to both a real increase of the TOA radiances and scattering due to the sensor. Part of the reason for the increase could also be that it is more likely to find a large, cloud-free area at nadir than at the edge of the scan (L_t is lower at nadir than at the edge of the scan by about 50%). It is not clear why the radiances are often lower at "Distance to cloud 20" versus "Distance to cloud 39," especially in the red and NIR. It is possible that the small number of pixels at large distances does not yield a representative sampling. Note that the MODIS Aqua cloud mask [covering two (three) pixels adjacent to a cloud in the track (scan) direction] excludes the steepest part of the curves from ocean color processing, eliminating the largest stray light effects.

Figure 11 also shows the results for SeaWiFS [3] data (MLAC data files S2003070224619 and S1999117171012). SeaWiFS has more sensor intrinsic stray light than MODIS Aqua, but a stray light

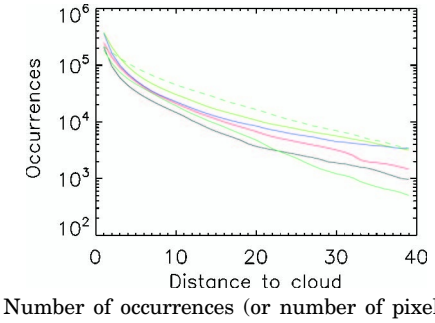

Fig. 10. Number of occurrences (or number of pixels) for each "Distance to cloud" in the investigated data files. The black, red, and blue curves are for Aqua granules A20030701810, A20030702305, and 20031271435, respectively. The green curves are for SeaWiFS MLAC data, files S2003070224619 and S1999117171012 (only scan lines 4712 to 7439 were used from the first file, lines 4512 to 7254 from the second file, and lines 10,000 to 12,900 from the second file (dashed curve).

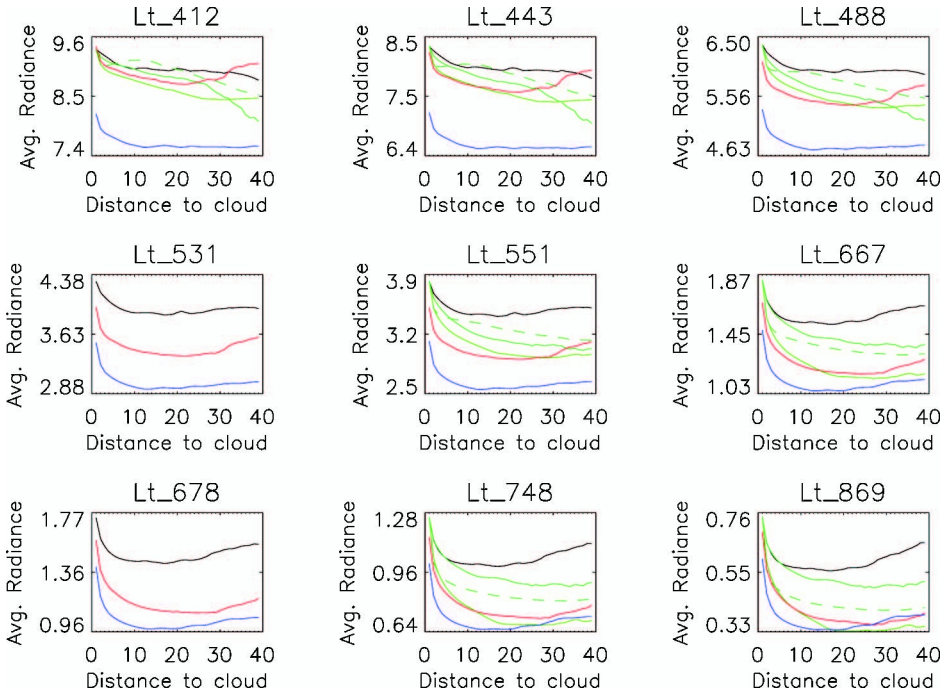

Fig. 11. Average TOA radiances for each set of pixels "Distance to cloud x" (with $1 \le x < 40$) for MODIS Aqua bands 8–16. Radiance unit is mW/(cm^2 sr μm). The black, red, and blue curves are for granules A20030701810, A20030702305, and 20031271435, respectively. The green curves are for SeaWiFS MLAC data; see caption of Fig. 10. To fit the plotting range, SeaWiFS radiances (bands 1–3 and 5–8) were normalized to the starting point of the black curve. MODIS bands 11 and 14 (531 and 678 nm) have no direct equivalent in SeaWiFS.

correction has been applied to the SeaWiFS data [22]. It can be seen that the results are qualitatively similar to MODIS Aqua, which suggests that, indeed, the features we see are mainly due to scattering processes in the atmosphere. Based on the very limited amount of data used in this study, it seems that the rise of L_t when approaching a cloud is steeper in Aqua than in SeaWiFS.

Figure 12 shows several ocean color products as a function of "Distance to cloud." It can be seen that

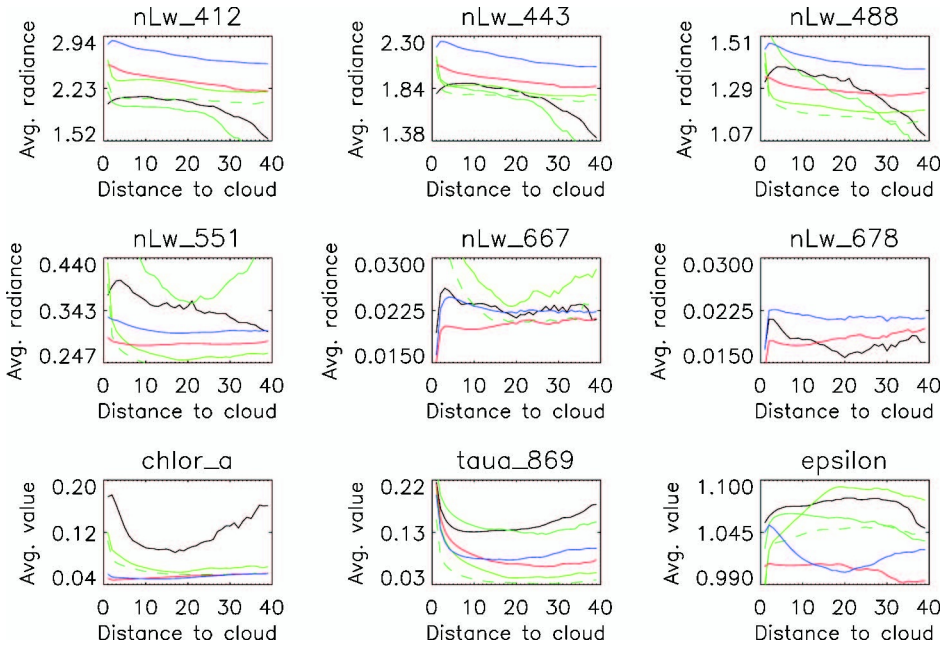

Fig. 12. Average ocean color products for each set of pixels "Distance to cloud x" (with $1 \le x < 40$) for MODIS Aqua and SeaWiFS. Water-leaving radiance (nLw) unit is mW/(cm^2 sr μm), chlorophyll unit is mg/m^3, AOT (taua) and epsilon are dimensionless. The black, red, and blue curves are for granules A20030701810, A20030702305, and 20031271435, respectively. The green curves are for SeaWiFS MLAC data; see caption of Fig. 10. The missing SeaWiFS line for chlorophyll is out of the plotting range (minimum value of that curve is 0.2, with a shape similar to the black curve).

there is a general trend of the water-leaving radiances to increase when approaching a cloud. The aerosol optical thickness (AOT) shows a drastic increase when approaching a cloud (which is expected), epsilon (the ratio of the aerosol reflectances of bands 15 and 16, see Gordon and Wang [23]) does not show a consistent behavior. The analysis of these results is still in progress. The variation among the curves in the chlorophyll plot suggests that many more granules are needed to derive an average trend. However, it is encouraging that the two MODIS curves for granules with deep water only (blue and red) are generally similar (the black curve is for the MODIS granule containing coastal regions and its pattern is clearly different from the blue and red curves, especially for chlorophyll).

7. Conclusions and Outlook

The PSF presented here requires further testing. We are planning to apply the correction approach from Zong *et al.*[9] to real MODIS data to quantify the effect of stray light on the retrieval of chlorophyll, water-leaving radiance, and AOT. Currently, a 5×7 mask is applied around cloud pixels (5 pixels in the track direction, 7 pixels in the scan direction; i.e., for a clear ocean scene contaminated by 1 cloudy pixel, 35 pixels are masked), which has significantly improved the agreement between the AOT of MODIS Aqua and the SeaWiFS sensor; see Franz *et al.* [3]. This mask indeed removes the steepest part of the L_t curves; see Fig. 11. However, it also excludes a large amount of data (about 50% of the ocean pixels) from the level 3 processing.

The effects of the MODIS PSF as simulated here are substantial. Even for a relatively small cloud (10×10 pixels; see Fig. 7), the stray light contamination 5 pixels away from the cloud is larger than the ocean color uncertainty goal of 0.5% [24]. We are not sure yet whether these effects are real or if they are largely due to an inaccurate characterization. In both cases, this underscores the need for a high-quality prelaunch stray light characterization for remote sensing ocean color sensors.

It is not obvious what level of stray light contamination is acceptable. In ocean color, errors that are spectrally correlated are much less harmful than those that are not. The spectral dependency of MODIS stray light contamination for ocean scenes is dominated by the high Lcloud/Ltyp ratio in the NIR; see Table 2. Figure 12 suggests that, without a stray light correction, the water-leaving radiances of MODIS Aqua decrease with increasing distance to the nearest cloud. This result is preliminary, but if confirmed, we expect a stray light correction algorithm to reduce this dependency.

It appears that the stray light contamination is about twice as high in MODIS Terra than in MODIS Aqua for band 11. It should be possible to confirm or disprove this result by analyzing MODIS Terra and Aqua images. However, MODIS Terra ocean color products have had severe accuracy issues [25], which make a comparison problematic. Recent improvements to the data quality [26] may enable such studies.

According to the simulated cloud images, band 13 has a far higher stray light contamination than band 14. The FLH algorithm is very sensitive to differences in bands 13 and 14. Therefore, the FLH algorithm may be a good tool to evaluate the usefulness of a stray light correction for MODIS Aqua.

We thank Roger Drake from SBRS/Raytheon, who provided the MODIS Aqua prelaunch characterization data (near-field response measurements), and Jim Young from SBRS/Raytheon for the Harvey–Shack modeling. Suggestions from the anonymous reviewers improved this manuscript. Several figures, both tables, and parts of the text have been previously published in [27].

References and Notes

1. W. L. Barnes, T. S. Pagano, and V. V. Salomonson, "Prelaunch characteristics of the Moderate Resolution Imaging Spectroradiometer (MODIS) on EOS-AM1," IEEE Trans. Geosci. Remote Sens. **36**, 1088–1100 (1998).
2. C. L. Parkinson, "Aqua: an Earth-Observing Satellite mission to examine water and other climate variables," IEEE Trans. Geosci. Remote Sens. **41**, 173–183 (2003).
3. B. A. Franz, P. J. Werdell, G. Meister, S. W. Bailey, R. E. Eplee, Jr., G. C. Feldman, E. J. Kwiatkowska, C. R. McClain, F. S. Patt, and D. Thomas, "The continuity of ocean color measurements from SeaWiFS to MODIS," Proc. SPIE **5882**, 58820W (2005).
4. E. Waluschka, S. Qiu, and G. D. Godden, "MODIS stray light simulation," Proc. SPIE **2864**, 350–360 (1996).
5. S. Qiu, G. Godden, X. Wang, and B. Guenther, "Satellite-Earth remote sensor scatter effects on Earth scene radiometric accuracy," Metrologia **37**, 411–414 (2000).
6. B. Guenther, G. D. Gooden, X. Xiong, E. J. Knight, S. Qiu, H. Montgomery, M. M. Hopkins, M. G. Khayat, and Z. Hao, "Prelaunch algorithm and data format for the Level 1 calibration products for the EOS-AM1 Moderate Resolution Imaging Spectroradiometer (MODIS)," IEEE Trans. Geosci. Remote Sens. **36**, 1142–1151 (1998).
7. C. Huang, J. R. G. Townshend, S. Liang, S. N. V. Kalluri, and R. S. DeFries, "Impact of sensor's point spread function on land cover characterization: assessment and deconvolution," Remote Sens. Environ. **80**, 203–212 (2002).
8. Y. Zong, S. W. Brown, B. C. Johnson, K. R. Lykke, and Y. Ohno, "Simple spectral stray light correction method for array spectroradiometers," Appl. Opt. **45**, 1111–1119 (2006).
9. Y. Zong, S. W. Brown, G. Meister, R. A. Barnes, and K. R. Lykke, "Characterization and correction of stray light in optical instruments," Proc. SPIE **6744**, 67441L (2007).
10. T. Hurt and P. Derrick, "MODIS FM1 near field response," Raytheon, Interdepartmental Correspondence, Ref. PL3095-N07729 Rev. A (2000).
11. P. Derrick, "MODIS FM1 Harvey–Shack scattering model analysis," Raytheon, Interdepartmental Correspondence, Ref. PL3095-N07881 (2002).
12. C. Morbey and J. B. Hutchings, "Telescope baffle performance for Lyman Far Ultraviolet Spectrographic Explorer," Appl. Opt. **32**, 3570–3584 (1993).
13. J. B. Young, "Point spread function (PSF) near field response measurement methodology—revision," SBRS internal memorandum, Ref. PL3095-N05401 (1995).

14. Although it may be possible to restrict the photon acquisition time of the detector to only the time when the detector FOV image falls exactly in the desired pixel boundary, this would result in a very short acquisition time, and, therefore, low signal-to-noise ratio (SNR). Allowing the detectors to acquire photons even when the FOV is not in the ideal position is a compromise between SNR and contrast resolution that was made during instrument design.
15. M. Nishihama, "MODIS Level 1A Earth location: algorithm theoretical basis document Version 3.0," NASA Goddard Space Flight Center (1997).
16. NASA, "Specifications for the Moderate Resolution Imaging Spectroradiometer (MODIS)," GSFC 422-20-02, Revision A (1993).
17. I. Koren, L. A. Remer, Y. J. Kaufman, Y. Rudich, and J. V. Martins, "On the twilight zone between clouds and aerosols," Geophys. Res. Lett. **34**, L08805 (2007).
18. J. Redemann, Q. Zhang, P. B. Russell, J. M. Livingston, and L. A. Remer, "Case studies of aerosol remote sensing in the vicinity of clouds," J. Geophys. Res. **114**, D06209 (2009).
19. T. Varnai and A. Marshak, "MODIS observations of enhanced clear sky reflectance near clouds," Geophys. Res. Lett. **36**, L06807 (2009).
20. J. C. Chiu, A. Marshak, Y. Knyazikhin, P. Pilewski, and W. J. Wiscombe, "Physical interpretation of the spectral radiative signature in the transition zone between cloud-free and cloudy regions," Atmos. Chem. Phys. **9**, 1419–1430 (2009).
21. K. Baith, R. Lindsay, G. Fu, and C. R. McClain, "SeaDAS, a data analysis system for ocean-color satellite sensors," EOS Trans. Am. Geophys. Union **82**, 202–205 (2001).
22. E. Yeh, R. Barnes, M. Darzi, L. Kumar, E. Early, B. Johnson, J. Mueller, and C. Trees, "Case Studies for SeaWiFS calibration and validation, Part 4," NASA, Goddard Space Flight Center 41, NASA Technical Memorandum 104566, SeaWiFS Technical Report Series (1997).
23. H. Gordon and M. Wang, "Retrieval of water-leaving radiance and aerosol optical thickness over the oceans with SeaWiFS: a preliminary algorithm," Appl. Opt. **33**, 443–452 (1994).
24. H. R. Gordon, T. Du, and T. Zhang, "Atmospheric correction of ocean color sensors: analysis of the effects of residual instrument polarization sensitivity," Appl. Opt. **36**, 6938–6948 (1997).
25. B. A. Franz, E. J. Kwiatkowska, G. Meister, and C. R. McClain, "Moderate Resolution Imaging Spectroradiometer on Terra: limitations for ocean color applications," J. Appl. Remote Sens. **2**, 023525 (2008).
26. E. J. Kwiatkowska, B. A. Franz, G. Meister, C. R. McClain, and X. Xiong, "Cross calibration of ocean-color bands from Moderate-Resolution Imaging Spectroradiometer on Terra platform," Appl. Opt. **47**, 6796–6810 (2008).
27. G. Meister, Y. Zong, and C. R. McClain , "Derivation of the MODIS Aqua point-spread function for ocean color bands," Proc. SPIE **7081**, 70811F (2008).